Received: 28 March 2022 | Revised: 21 June 2022 | Accepted: 24 June 2022 | Published on: 22 July 2022

DOI: 10.1002/joc.7777

RESEARCH ARTICLE

International Journal of Climatology RMetS

Modulation of western North Pacific tropical cyclone formation by central Pacific El Niño–Southern Oscillation on decadal and interannual timescales

Jinjie Song[1,2] | **Philip J. Klotzbach**[3] | **Na Wei**[1,2] | **Yihong Duan**[2]

[1]Nanjing Joint Institute for Atmospheric Sciences, Chinese Academy of Meteorological Sciences, Nanjing, China

[2]State Key Laboratory of Severe Weather, Chinese Academy of Meteorological Sciences, Beijing, China

[3]Department of Atmospheric Science, Colorado State University, Fort Collins, Colorado, USA

Correspondence
Yihong Duan, State Key Laboratory of Severe Weather, Chinese Academy of Meteorological Sciences, 46 Zhongguancun South Avenue, Beijing 100081, China.
Email: duanyh@cma.gov.cn

Funding information
National Natural Science Foundation of China, Grant/Award Numbers: 41905001, 42175007, 42192552, 61827901; G. Unger Vetlesen Foundation; China Postdoctoral Science Foundation, Grant/Award Number: 2020M680789

Abstract

This study investigates the impact of central Pacific (CP) El Niño–Southern Oscillation (ENSO) on tropical cyclone (TC) frequency over the western North Pacific (WNP) on decadal and interannual timescales. The CP ENSO-TC frequency relationship is strong and significant only on decadal timescales, with enhanced TC formation over most of the WNP associated with warm CP ENSO phases. TC formation changes, driven by CP ENSO, exhibit a southeast–northwest dipole pattern on interannual timescales, similar to the typical pattern induced by eastern Pacific ENSO. Associated with warm CP ENSO phases on decadal timescales are increases in TC formation east of 125°E, while increases in TC formation east of 140°E are observed with warm CP ENSO phases on interannual timescales. These increases in TC activity are primarily caused by favourable dynamic conditions, including increased 850-hPa relative vorticity and 200-hPa divergence and decreased 850–200-hPa vertical wind shear. The main TC formation difference on decadal and interannual timescales is concentrated over the longitudinal band of 125°–140°E, where reduced TC formation is observed on interannual timescales during CP El Niño years, predominately due to suppressed thermodynamic factors, for example, reduced maximum potential intensity and 700–500-hPa relative humidity. We find insignificant (significant) changes in thermodynamic conditions between 125°E and 140°E due to weak (strong) descending motion in the western cell of the anomalous Walker circulation on decadal (interannual) timescales. This can be explained by different patterns of CP ENSO-induced sea surface temperature anomalies on different timescales.

KEYWORDS
central Pacific ENSO, tropical cyclone, western North Pacific

1 | INTRODUCTION

El Niño–Southern Oscillation (ENSO) is often considered to be the dominant factor modulating tropical cyclone (TC) activity over the western North Pacific (WNP) on timescales ranging from a few months to several years (Emanuel, 2018). Traditionally, ENSO can be classified into two flavours: eastern Pacific (EP) ENSO (also known as conventional ENSO, canonical ENSO or cold tongue ENSO) with maximum oceanic warming/cooling over the eastern equatorial Pacific, and central Pacific (CP) ENSO (also known as ENSO Modoki or warm pool ENSO) with sea surface temperature (SST) variability centred over the central equatorial Pacific (Kao and Yu, 2009; Capotondi *et al*., 2015; Timmermann *et al*., 2018).

Although EP ENSO does not significantly impact basinwide WNP TC frequency, it significantly modulates average TC formation location (Chan, 1985; 2000; Lander, 1994; Saunders *et al*., 2000; Wang and Chan, 2002; Li and Zhou, 2012). WNP TCs, on average, form more equatorward and eastward during EP El Niño years, due to more conducive environmental conditions including warmer SSTs, greater mid-level relative humidity and lower vertical wind shear (VWS) over the southeastern quadrant of the WNP relative to EP La Niña years. Compared with EP ENSO, CP ENSO more significantly modulates WNP TC activity, especially the formation of WNP TCs (Chen and Tam, 2010; Kim *et al*., 2011; Zhang *et al*., 2015; Patricola *et al*., 2018). There is a significant positive correlation between basinwide WNP TC frequency and the CP ENSO index (Chen and Tam, 2010). During CP El Niño, TC formation is enhanced over most of the WNP, due to a large-scale anomalous cyclonic circulation, anomalous ascending motion, as well as an anomalously moist mid-troposphere in response to the maximum oceanic warming over the central Pacific (Chen and Tam, 2010; Kim *et al*., 2011; Patricola *et al*., 2018). During CP La Niña, the changes in both TC formation and the large-scale environment show nearly a mirror image of those during CP El Niño (Wang *et al*., 2013; Li and Wang, 2014).

Liu and Chen (2018) noted an abrupt change in the relationship between CP ENSO and WNP TC formation in the early 1990s, with an insignificant relationship from 1950 to 1990 and a significant relationship from 1991 to 2011. They attributed this feature to interdecadal changes in the spatiotemporal variability of CP ENSO. Since ~1990, CP ENSO-induced SST variations covered a larger portion of the central Pacific, resulting in an intensified and northwestward-expanded anomalous cyclonic (anticyclonic) circulation over the WNP during CP El Niño (CP La Niña). They further linked these changes to anthropogenic global warming, which induced a CP El Niño-like warming in the Pacific as well as an increasing proportion of CP ENSO events to EP ENSO events. Furthermore, Song *et al*. (2021) found that the impact of CP ENSO on WNP TC formation experienced decadal changes during the past few decades. The correlation between the CP ENSO index and basinwide WNP TC frequency was weak from 1975 to 1989, became strong and significant from 1990 to 2004 and became weak again from 2005 to 2019. They found that this relationship primarily resulted from changes in the SST distribution related to CP ENSO. CP ENSO in 1990–2004 was characterized by a tripole SST pattern with maximum SST anomalies (SSTAs) in the equatorial central Pacific, while maximum SSTAs were located over the subtropical northeastern Pacific in 1975–1989 and 2005–2019.

Sullivan *et al*. (2016) reported that CP El Niño represented a dominant spectral peak on decadal timescales with comparatively weak power on interannual timescales. They found distinct distributions of SST changes for interannual and decadal components of CP El Niño. For the interannual component, there were positive SSTAs over the equatorial central-to-eastern Pacific, covering the Niño1+2 region. By comparison, for the decadal component, positive SSTAs were found from the subtropical northeastern Pacific to the equatorial central Pacific, while negative SSTAs were observed in the Niño1+2 region.

The SSTA pattern of the interannual (decadal) CP El Niño component is very similar to that of El Niño Modoki I (II) events identified by Wang and Wang (2013). For El Niño Modoki I events, positive SSTAs first developed over the equatorial central Pacific and then gradually intensified. For El Niño Modoki II events, positive SSTAs first developed over the subtropical northeastern Pacific and then extended into the equatorial central Pacific. Wang and Wang (2013) also found different TC tracks in response to El Niño Modoki I and El Niño Modoki II. In contrast to El Niño Modoki I, El Niño Modoki II was associated with northwesterly anomalies in TC steering flow, reducing the number of TCs making landfall in China. This was further linked to a westward extension of the western Pacific subtropical high (WPSH) for El Niño Modoki I and an eastward retreat of the WPSH for El Niño Modoki II.

In addition, Stuecker (2018) showed a tight connection between the Pacific Meridional Mode (PMM) and CP ENSO, with the positive (negative) phase of the PMM often corresponding to CP El Niño (CP La Niña). Liu *et al*. (2019) recently revisited the statistical relationship between the PMM and TC formation over the southeastern part of the WNP (0°–20°N, 140°E–180°). They found that the significant relationship between the PMM and TC formation frequency over the southeastern WNP was dominated by their covariability on decadal timescales,

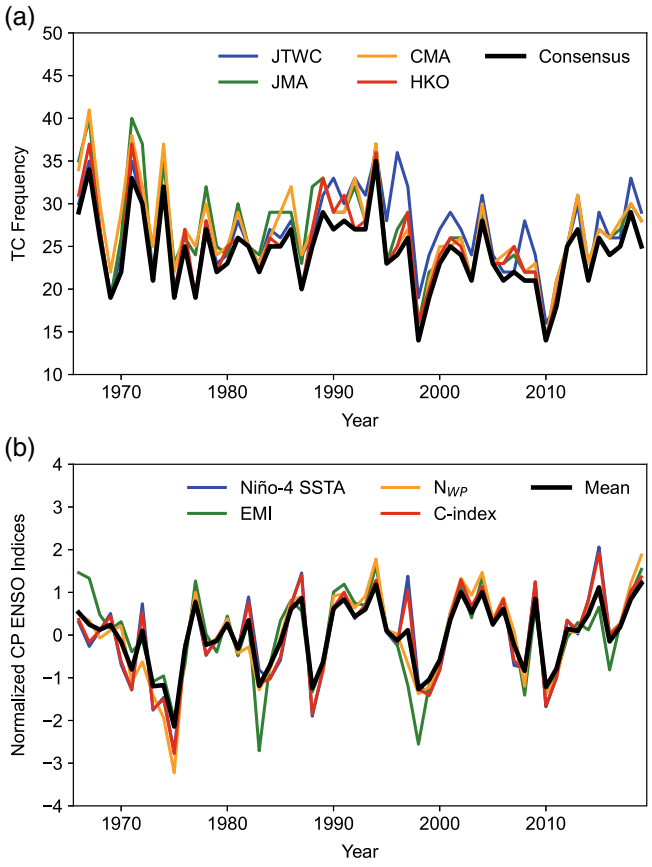

FIGURE 1 Time series of (a) WNP TC frequency and (b) the CP ENSO index during June–November for the period of 1966–2019. In (a), blue, green, orange and red lines denote WNP TC frequencies obtained from the JTWC, JMA, CMA and HKO best-track datasets, respectively. The black line refers to the frequency of TCs simultaneously recorded in all four datasets. In (b), blue, green, orange and red lines denote the normalized time series of Niño4 SSTA, EMI, N_{WP} and the C-index, respectively. The black line displays the arithmetic mean of these four indices

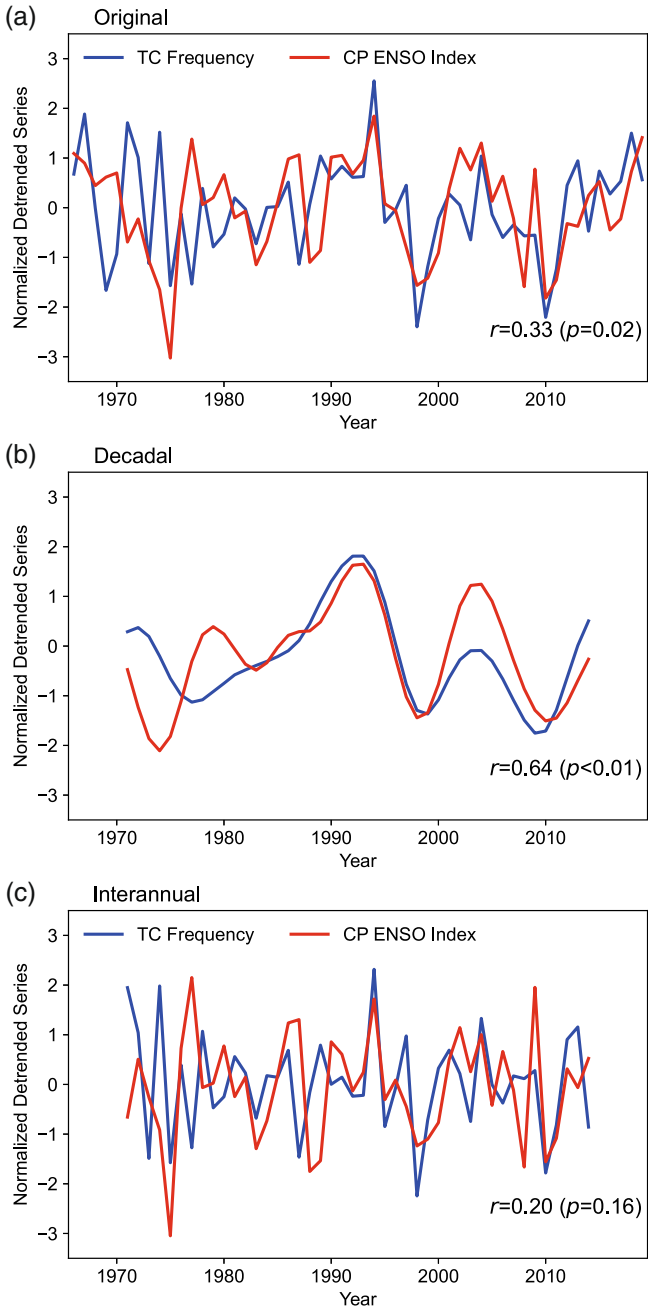

FIGURE 2 Normalized detrended series of (a) original, (b) decadal and (c) interannual WNP TC frequency and the CP ENSO index. The timespan is 1966–2019 in (a), while it is 1971–2014 in (b, c), which excludes the first and last 5 years of the period from 1966–2019 owing to the 11-year Gaussian filtering

while the correlation between the PMM and southeastern WNP TC formation was not significant on interannual timescales.

Given these prior studies, it is likely that CP El Niño modulates WNP TC activity differently on interannual and decadal timescales. Therefore, we re-examine the relationship between CP ENSO and WNP TC formation by separating the relationship into its interannual and decadal components. The remainder of this study is arranged as follows. Section 2 describes the data and analysis methods. Sections 3 and 4 discuss the influences of CP ENSO on WNP TC formation and large-scale environmental conditions, respectively. Section 5 provides an analysis of the mechanisms likely driving the different influences of CP ENSO on WNP TC activity on different timescales. A conclusion is given in section 6.

2 | DATA AND METHODS

WNP TC best track data for the period of 1966–2019 are taken from the International Best Track Archive for Climate Stewardship (IBTrACS) v4 dataset (Knapp *et al.*, 2010). This study focuses on the TC-active season over the WNP from June to November, with approximately 85% of annual WNP TCs occurring during this period

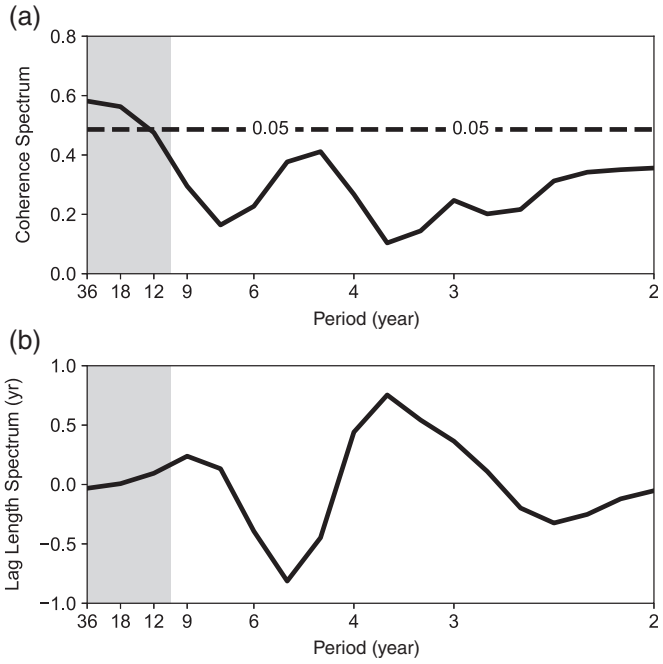

FIGURE 3 (a) Coherence spectrum and (b) lag length spectrum between the CP ENSO index and WNP TC frequency. Grey areas denote periods longer than 10 years. The horizontal dashed line in (a) refers to the 0.05 significance level based on an *F* test

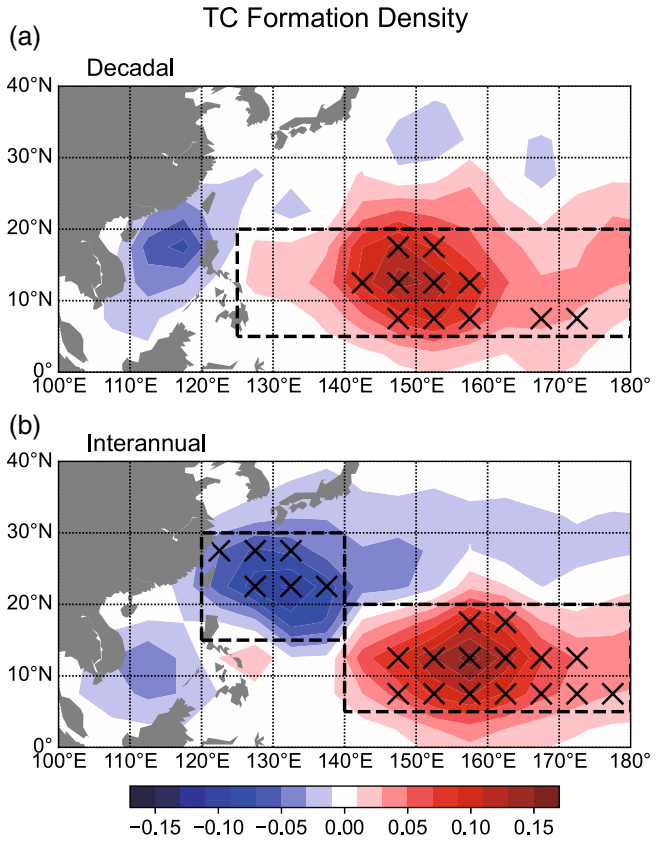

FIGURE 4 Regressions of WNP TC formation density on the normalized (a) decadal and (b) interannual CP ENSO indices during 1971–2014. Black crosses denote regressions significant at the 0.05 level based on a two-tailed Student's *t* test

(Song and Klotzbach, 2019). There are four warning agencies operationally providing TC best tracks over the full WNP. These agencies are the Joint Typhoon Warning Center (JTWC), the Japan Meteorological Agency (JMA), the China Meteorological Administration (CMA) and the Hong Kong Observatory (HKO). To reduce the uncertainty among data sources and enhance the robustness of the results, this study only considers TC cases simultaneously recorded by all four agencies, as suggested by Song and Klotzbach (2018). This approach naturally excludes weak TCs, since the JMA does not record tropical depressions in its best track data. Figure 1a shows the annual time series of WNP TC frequency during June–November from these four different agencies, in which only TCs with a lifetime maximum intensity reaching tropical storm intensity (maximum sustained wind ≥34 kt) are considered for JTWC, CMA and HKO. The annual frequency of TCs simultaneously recorded by all agencies is highly correlated with those recorded by individual agencies. Additionally, the TC formation location is identified as the first record that is simultaneously listed by all four aforementioned agencies, similar to Song and Klotzbach (2018). The TC formation density is first obtained by counting TC formation numbers over a 5° × 5° grid and is then spatially smoothed through the method proposed by Kim *et al.* (2011).

Monthly mean SST data over a 1° × 1° grid are provided by the Hadley Centre Sea Ice and Sea Surface Temperature dataset (HadISST; Rayner *et al.*, 2003). Several SST-based indices have been introduced to identify CP ENSO, including the Niño4 SSTA (Yeh *et al.*, 2009; Kug *et al.*, 2010), the ENSO Modoki index (EMI; Ashok *et al.*, 2007), the N_{WP} index (Ren and Jin, 2011) and the C-index (Takahashi *et al.*, 2011). The EMI is defined as

$$\mathrm{EMI}=\overline{\mathrm{SSTA}}_{\mathrm{C}}-0.5\times\overline{\mathrm{SSTA}}_{\mathrm{E}}-0.5\times\overline{\mathrm{SSTA}}_{\mathrm{W}}, \quad (1)$$

where the overbar represents the area-averaged SSTA, which is calculated over the three regions specified as the central (C: 165°E–140°W, 10°S–10°N), eastern (E: 110°–70°W, 15°S–5°N) and western (W: 125°–145°W, 10°S–20°N) tropical Pacific.

The N_{WP} index is defined as

$$\mathrm{N_{WP}}=\mathrm{SSTA_{Niño4}}-\alpha\times\mathrm{SSTA_{Niño3}},\qquad \alpha=\begin{cases}0.4, \mathrm{SSTA_{Niño4}}\times\mathrm{SSTA_{Niño3}}>0\\ 0, \text{otherwise}\end{cases}. \quad (2)$$

The C-index is defined as

$$\mathrm{C}=1.7\times\mathrm{SSTA_{Niño4}}-0.1\times\mathrm{SSTA_{Niño1+2}}. \quad (3)$$

As shown in Figure 1b, there are significant temporal correlations among these CP ENSO indices, consistent

with Jeong and Ahn (2017). We thus use the arithmetic mean of the normalized time series of these indices to represent CP ENSO. An 11-year Gaussian filter is performed on the annual detrended time series of this mean CP ENSO index during June–November to separate the CP ENSO index into its interannual and decadal components.

There are several large-scale environmental variables that can influence TC formation including maximum potential intensity (MPI), 700–500-hPa relative humidity (RHMD), 850-hPa relative vorticity (VOR850), 200-hPa divergence (DIV200) and 850–200-hPa VWS (Liang *et al.*, 2021; Cai *et al.*, 2022; Li *et al.*, 2022; Ma and Fei, 2022; Zhao *et al.*, 2022a; 2022b). All of these parameters are calculated from the fifth generation European Centre for Medium-Range Weather Forecasts (ECMWF) reanalysis of the global climate (ERA5; Hersbach *et al.*, 2020), with a horizontal resolution of 0.25° × 0.25°.

Statistical significance of correlation coefficients and regression coefficients is estimated based on a 2-tailed Student's *t* test. In the test, the effective sample size proposed by Bretherton *et al.* (1999) is applied to the original time series and their interannual and decadal components. A cross-spectral analysis is used to show the relationship between the two time series for different periods, while the significance level of the coherence is determined by an *F* test.

3 | RELATIONSHIP BETWEEN CP ENSO AND WNP TC FREQUENCY

Consistent with Chen and Tam (2010), we find a significant positive correlation between the CP ENSO index and basinwide TC frequency over the WNP during 1966–

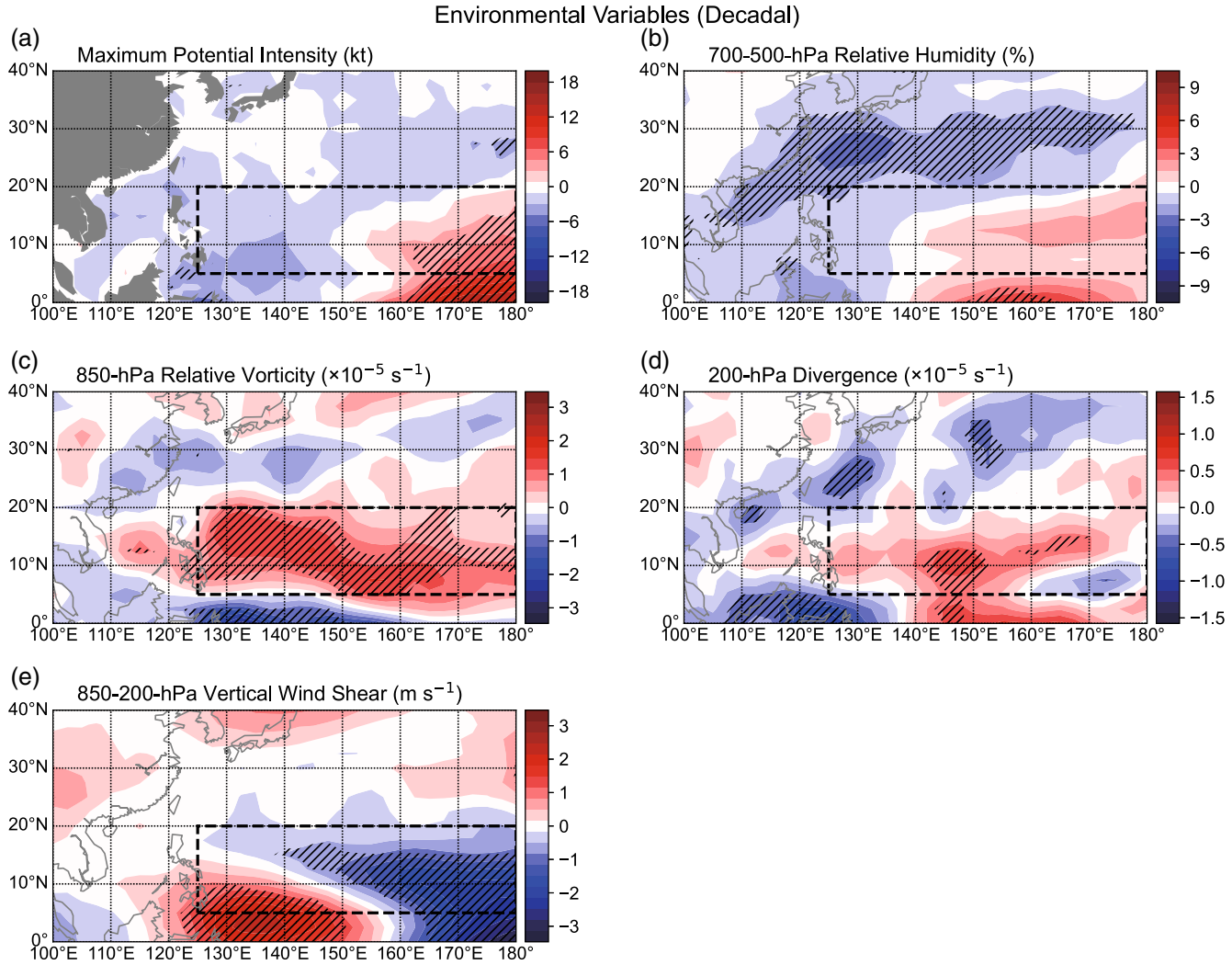

FIGURE 5 Regressions of (a) MPI, (b) RHMD, (c) VOR850, (d) DIV200 and (e) VWS on the normalized decadal component of CP ENSO during 1971–2014. Hatched regions refer to regressions significant at the 0.05 level based on a two-tailed Student's *t* test

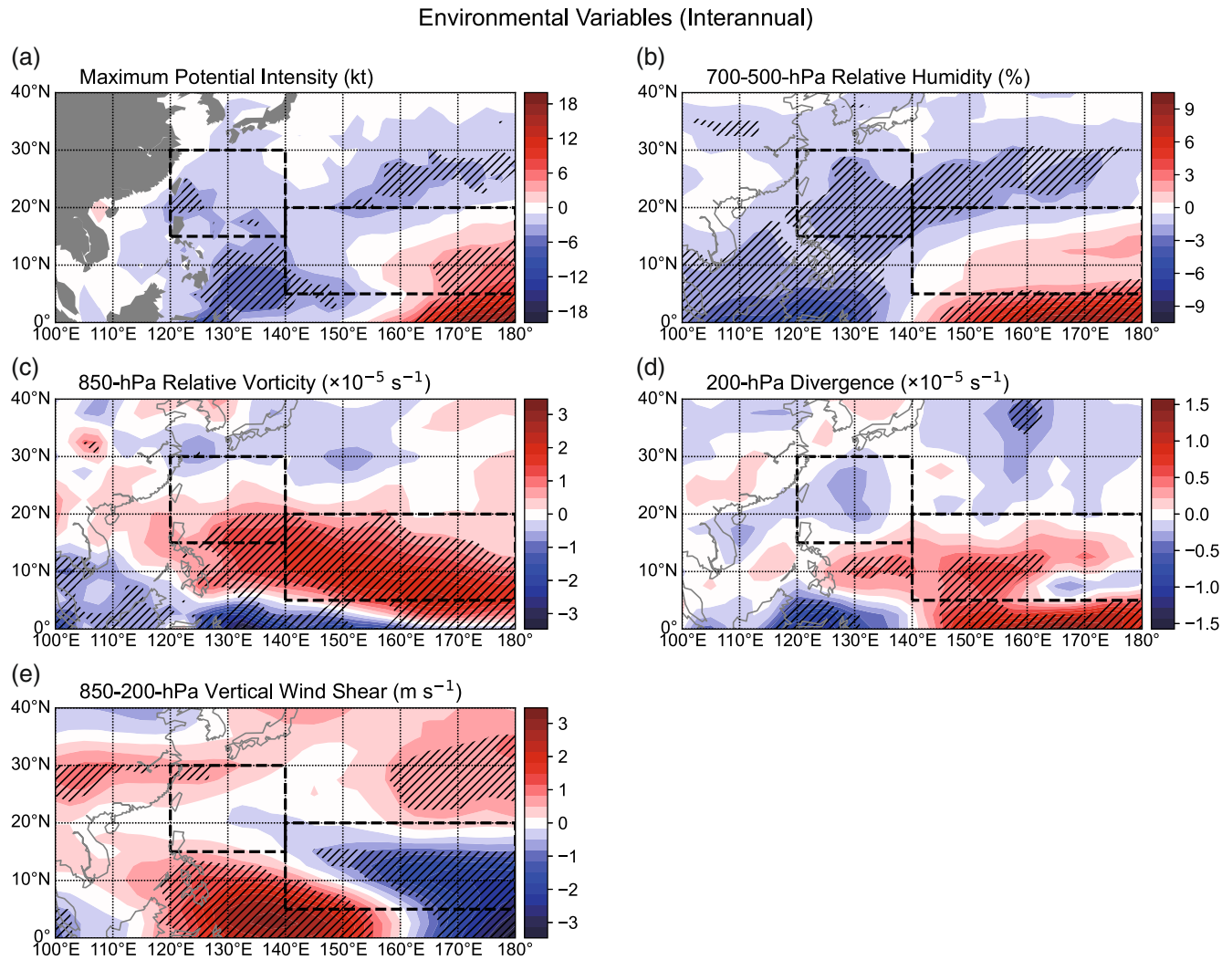

FIGURE 6 As in Figure 5, but for regressions on the normalized interannual component of CP ENSO

2019 ($r = .33$, $p = .02$) (Figure 2a). Figure 2b,c also displays the CP ENSO–WNP TC frequency relationship on different timescales. CP ENSO and WNP TC frequency shows significant coherence only on periods longer than 10 years, indicating a significant relationship on decadal timescales (Figure 3a). Although a coherence peak is shown in the 4–6 year period, which corresponds to a typical ENSO cycle, it is not statistically significant. Moreover, the CP ENSO–WNP TC frequency relationship is almost simultaneous on decadal timescales, since the lag length is shorter than 0.5 years (Figure 3b).

Due to distinct relationships between CP ENSO and WNP TC frequency on different timescales, the original time series are separated into decadal and interannual components after removing the long-term linear trends. Figure 2b displays highly coherent variations in the decadal components of CP ENSO and WNP TC frequency ($r = .64$, $p < .01$), particularly during the timespan from the mid-1980s to the late 2000s. Both CP ENSO and TC frequency show opposite variations between the 1970s and the mid-1980s, with CP ENSO changing from a warm phase to a cold phase and TC frequency changing from fewer TCs to more TCs. Due to this, the decadal CP ENSO–TC frequency relationship undergoes decadal changes and is relatively weak before the 1990s (figure not shown). The correlation between the decadal components of TC frequency and the CP ENSO index is 0.01 ($p = .96$) during 1971–1989 and 0.82 ($p < .01$) during 1990–2004. Additionally, there is a time lag between CP ENSO and TC frequency since the late 2000s. Despite these changes in the relationship, there is a significant correlation ($r = .62$, $p = .04$) between the decadal components of TC frequency and the CP ENSO index during 2005–2014.

By contrast, Figure 2c shows a weak correlation between the interannual components of CP ENSO and

WNP TC frequency (r = .20, p = .16). The correlations are −0.05 (p = .85), 0.70 (p < .01) and 0.47 (p = .15) in 1971–1989, 1990–2004 and 2005–2014, respectively. Consistent with Song *et al.* (2021), the interannual relationship between CP ENSO and TC frequency is only strong and significant from the 1990s to the mid-2000s, when most CP El Niño years were identified in previous publications (Kim *et al.*, 2011; Hsu *et al.*, 2013; Patricola *et al.*, 2018). The following results are not significantly changed if the study period is shortened to 1990–2014 (figures not shown).

Correspondingly, the spatial features of WNP TC formation as modulated by CP ENSO exhibit differences on decadal and interannual timescales (Figure 4). On decadal timescales, changes in TC formation density induced by CP El Niño show an east–west pattern, with enhanced (suppressed) TC formation east (west) of 125°E (Figure 4a). The enhancement of TC formation is observed over almost the entire WNP except the South China Sea (SCS). This enhancement is especially pronounced over the domain of 5°–20°N and 125°–180°E (Region A). This leads to a basinwide increase in WNP TC frequency during warm decades of CP ENSO. Note that most of Region A coincides with the study area in Liu *et al.* (2019), where CP ENSO and TC frequency showed a significant decadal correlation.

On interannual timescales, CP ENSO causes a southeast–northwest dipole pattern in anomalous TC formation density (Figure 4b). During warm phases of CP ENSO, enhanced TC formation is located over the region of 5°–20°N, 140°E–180° (Region B), while suppressed TC formation is concentrated over the region of 15°–30°N, 120°–140°E (Region C) and over the southern SCS. Compared with the decadal pattern, the interannual modulation of TC formation by CP El Niño retreats eastward, while the region with decreased TC formation extends northeastward. This feature is quite similar to the typical pattern of EP ENSO-induced TC formation changes (Kim *et al.*, 2011; Patricola *et al.*, 2018). Given the opposite changes in TC formation over the southeastern and northwestern quadrants of the WNP, there is only a weak interannual linkage between CP ENSO and basinwide TC frequency.

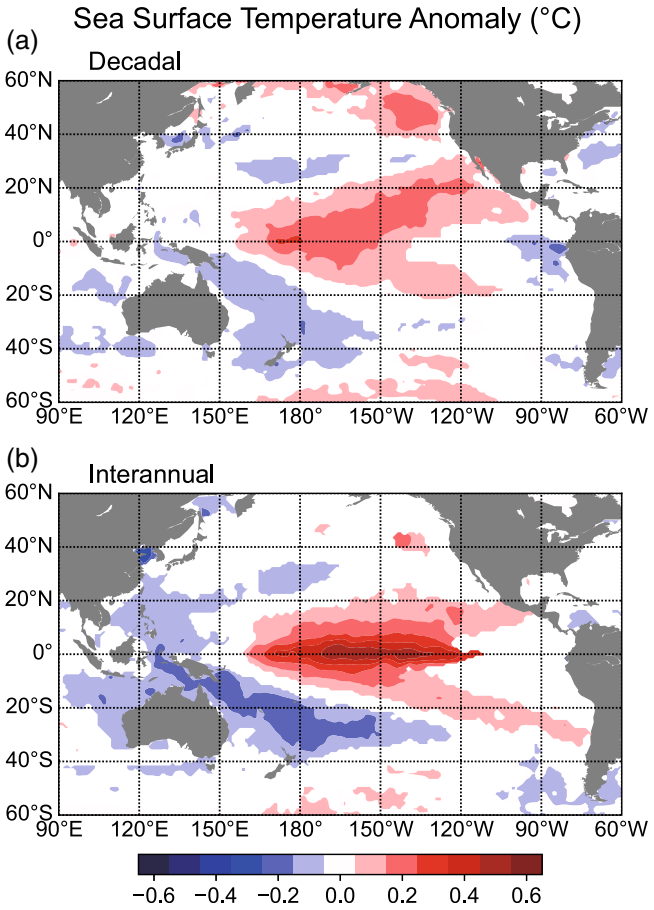

FIGURE 7 Regression of SSTA on the normalized decadal and interannual components of CP ENSO during 1971–2014. Only regressions significant at the 0.05 level based on a two-tailed Student's t test are shown

4 | ENVIRONMENTAL CHANGES ON DIFFERENT TIMESCALES

Figure 5 displays changes in environmental variables as modulated by CP ENSO on decadal timescales. Two thermodynamic factors (MPI and RHMD) both exhibit similar patterns to the CP El Niño-induced SSTA distribution, with positive anomalies over the equatorial central Pacific and negative anomalies from the tropical western Pacific to the subtropical central Pacific (Figure 5a,b). Significantly increased MPI is only observed east of 160°E and south of 15°N, favouring TC formation over the southeastern corner of Region A (Figure 5a). For RHMD, there are significant increases near the equator and significant decreases north of 20°N, with only weak changes over Region A (Figure 5b). These results imply that RHMD modulation by CP ENSO has only a minor impact on TC formation on decadal timescales.

By comparison, dynamic factors (VOR850, DIV200 and VWS) play a more important role than thermodynamic factors do. There are significant increases in VOR850 over almost all of Region A (Figure 5c), while significant increases in DIV200 are observed over the central part of Region A (Figure 5d). VWS is significantly weakened over most of Region A, except the southwestern quadrant where VWS is significantly strengthened (Figure 5e). As shown in Figure 4a, significant TC formation density increases are concentrated over the central-to-eastern part of Region A (140°E–180°), which is

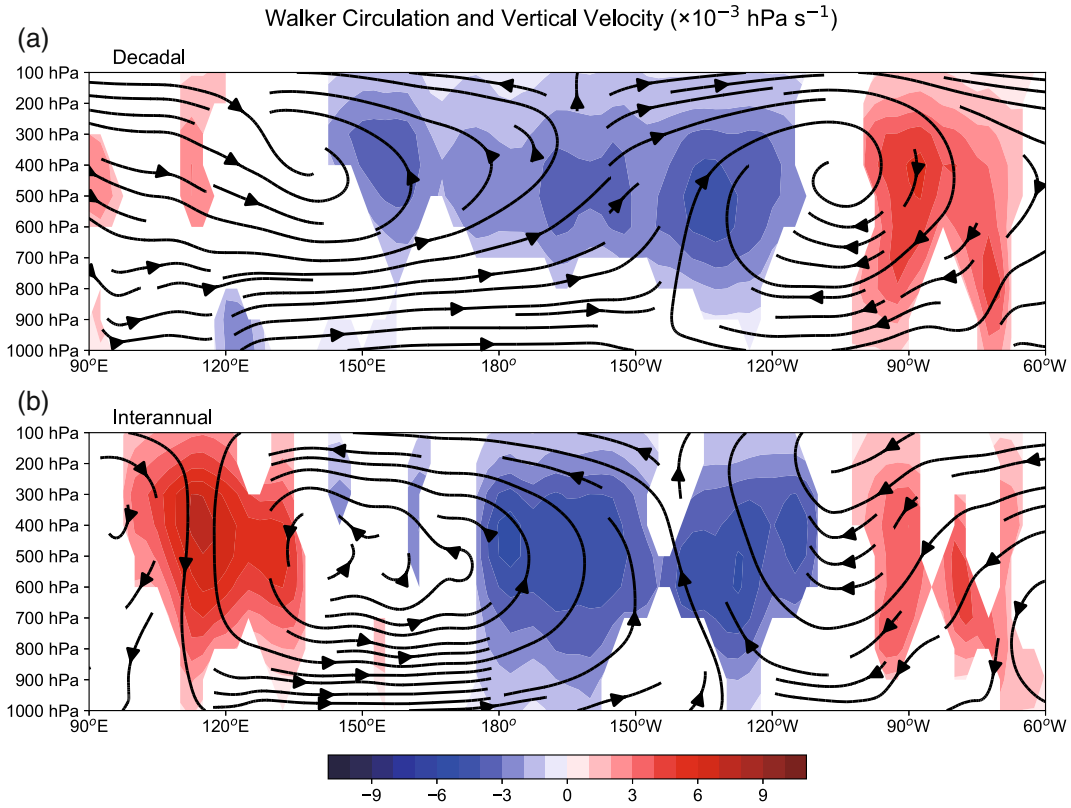

FIGURE 8 Regressions of vertical velocity and vertical circulation averaged between the equator and 10°N on the normalized decadal and interannual components of CP ENSO during 1971–2014. Streamlines are plotted after multiplying vertical velocity regressions by 500 at each pressure level. Only vertical velocity regressions significant at the 0.05 level based on a two-tailed Student's *t* test are shown

primarily linked to enhanced VOR850 and DIV200 and weakened VWS. Over the western part of Region A (125°–140°E), the influences of enhanced VOR850 and VWS oppose each other, leading to only weak increases in TC formation density.

Figure 6 displays changes in environmental variables modulated by CP ENSO on interannual timescales. Interestingly, the patterns of environmental changes induced by CP ENSO on interannual timescales are quite similar to those on decadal timescales, especially the spatial distributions of dynamic factor changes. However, there are obvious differences in the magnitude of thermodynamic variable changes on different timescales (Figure 6a,b). Although the spatial pattern of MPI and RHMD anomalies on interannual timescales remain nearly the same as on decadal timescales, their magnitudes are strengthened over most of the WNP. In particular, the reductions of MPI and RHMD on interannual timescales become significant south of 20°N and west of 140°E. Over this area, the favourable effects of increased VOR850 and DIV200 are offset by the suppressing effect of decreased MPI and RHMD and increased VWS (Figure 6), leading to little change in TC formation density.

Over Region B, the enhancement of TC formation is primarily caused by changes in dynamic factors, such as decreased VWS and increased VOR850 and DIV200 (Figure 6c–e). MPI changes likely play a secondary role, since they only exhibit significant increases east of 165°E (Figure 6a). By contrast, over Region C, thermodynamic variables have a more dominant impact on modulating TC formation than dynamic variables do. Reduced TC formation mainly arises from the suppressing effect of reduced MPI and RHMD, which surpasses the favouring effect of enhanced VOR850 (Figure 6a–c).

In summary, the difference in CP ENSO-induced TC formation anomalies on different timescales is primarily caused by the different changes in thermodynamic conditions (e.g., MPI and RHMD) over the WNP, particularly over the area east of 140°E.

5 | POSSIBLE MECHANISMS

Figure 7 displays SSTAs regressed on the normalized CP ENSO index on decadal and interannual timescales. Consistent with Sullivan *et al.* (2016), although the patterns

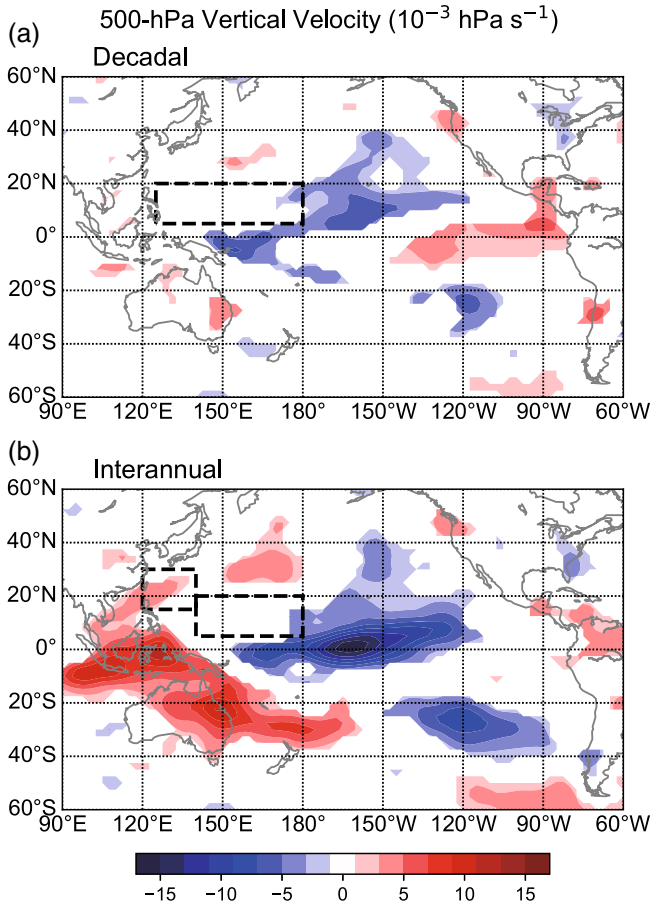

FIGURE 9 Regression of 500-hPa vertical velocity on the normalized decadal and interannual components of CP ENSO during 1971–2014. Only regressions significant at the 0.05 level based on a two-tailed Student's *t* test are shown

of CP ENSO-induced SSTA changes on both timescales show peak SST warming over the equatorial central Pacific, the details of the spatial patterns of the anomalies are somewhat different. On decadal timescales, positive SSTAs extend from the subtropical northeastern Pacific to the equatorial central Pacific (Figure 7a). Negative SSTAs are observed over the extreme eastern part of the tropical Pacific, while almost no significant SSTA changes are found over the western Pacific. By comparison, on interannual timescales, the SST warming over the equatorial central Pacific is much stronger than that on decadal timescales, while the warming extends eastward to the equatorial eastern Pacific (Figure 7b). There are no significant SSTA changes over the far eastern tropical Pacific, while there are negative SSTAs over the western Pacific. These far eastern tropical Pacific and western Pacific SSTA anomaly patterns are nearly opposite to those on decadal timescales.

Different SSTA distributions can lead to different changes in the Walker circulation, as shown in Figure 8. The anomalous Walker circulation shows a typical two-cell structure on both timescales, with ascending motion over the central Pacific and descending motion over the eastern and western Pacific. On decadal timescales, the strength of the eastern cell is much greater than that of the western cell (Figure 8a), as a result of more significant negative SSTAs over the eastern Pacific than over the western Pacific. Over the WNP, descending motion is only found east of 120°E, while there are almost no changes in vertical motion between 120°E and 140°E. By contrast, the western cell is much stronger than the eastern cell on interannual timescales (Figure 8b), due to more significant negative SSTAs over the western Pacific than over the eastern Pacific. Descending motion on interannual timescales dominates a large area from 100°E to 140°E, with a much greater magnitude than that on decadal timescales. Although the locations of anomalous ascending (descending) motion in Figure 8 do not exactly correspond to the locations of positive (negative) SSTA in Figure 7, the spatial pattern of regressed SSTAs is generally similar to that of regressed 500-hPa vertical velocity, on both decadal or interannual timescales (Figure 9).

On decadal timescales, significant anomalous descending motion is observed in the eastern Pacific, while there is only weak anomalous descending motion west of 120°E (Figure 9a). Over Region A, weak changes in vertical motion do not significantly influence vertical transport of moisture, leading to small changes in mid-level humidity. These small anomalies, plus a small reduction in SST, result in insignificant changes in MPI. By contrast, on interannual timescales, there is significant anomalous descending motion west of 140°E, while the anomalous descending motion over the eastern Pacific is almost negligible (Figure 9b). Over Region B, there are also weak changes in vertical motion, inducing minor SST and RHMD changes. Nonetheless, over Region C, strong descending motion suppresses the upward transport of moisture from the underlying ocean, resulting in significant decreases in humidity. Also given the significant negative SSTAs, there is a significant reduction in MPI.

6 | CONCLUSIONS

This study investigates the relationship between CP ENSO and WNP TC frequency on different timescales during June–November from 1966 to 2019. Although WNP TC frequency has been shown to significantly correlate with CP ENSO, we find that WNP TC frequency exhibits different correlations with CP ENSO on decadal and interannual timescales. The CP ENSO–WNP TC

frequency relationship is strong and significant on decadal timescales, while it is weak and insignificant on interannual timescales. On decadal timescales, there is enhanced TC formation east of 125°E and suppressed TC formation west of 125°E associated with CP El Niño. By comparison, a southeast–northwest dipole pattern in TC formation changes occurs on interannual timescales, with enhanced (suppressed) TC formation over the southeastern (northwestern) quadrants of the WNP. This feature is quite similar to the typical pattern of EP ENSO-induced TC formation changes.

The changes in WNP TC formation can be explained by changes in large-scale environmental variables induced by CP ENSO on both timescales. Although the patterns of regressions of environmental variables for the decadal CP ENSO component are quite similar to those for the interannual CP ENSO component, the regions of significance differ on decadal and interannual timescales. On decadal timescales, TC formation increases east of 125°E are primarily caused by favourable dynamic conditions, including increased VOR850 and DIV200 and decreased VWS. Increased MPI likely only has an impact east of 160°E. On interannual timescales, similar changes in dynamic conditions occur, resulting in enhanced TC formation over the region of 5°–20°N, 140°E–180°. By contrast, suppressed TC formation over the region of 15°–30°N, 120°–140°E is mainly caused by TC-unfavourable thermodynamic conditions, for example, reduced MPI and RHMD, while having only weak links to changes in dynamic factors. Given these findings, we conclude that the difference between TC formation changes induced by CP ENSO on different timescales is mainly concentrated over the longitudinal band of 125°–140°E.

We find different SSTA configurations for the decadal and interannual components of CP El Niño. On decadal timescales, significant positive SSTAs extend from the subtropical northeastern Pacific to the equatorial central Pacific, while significant negative SSTAs are observed over the far eastern tropical Pacific. On interannual timescales, significant positive SSTAs extend eastward to the equatorial eastern Pacific, while there are significant negative SSTAs over the western Pacific. This SSTA configuration leads to the eastern cell of the anomalous Walker circulation being weaker (stronger) than the western cell on decadal (interannual) timescales. On decadal timescales, due to weak descending motion from 125°E to 140°E, there are insignificant changes in vertical moisture transport, inducing minor changes in humidity. On interannual timescales, descending motion is relatively strong from 125°E to 140°E, suppressing vertical transport of water from the underlying ocean. This suppression of vertical transport can reduce atmospheric moisture and lead to a significant reduction of MPI and RHMD.

Many previous studies (e.g., Chen and Tam, 2010; Patricola *et al*., 2018) simulated the CP ENSO effect on WNP TC activity only by modifying SSTAs over the central equatorial Pacific. Our results highlight that this effect can be modulated if CP ENSO exhibits different SSTAs over the western and eastern Pacific. When CP ENSO occurs, it is necessary to monitor SST changes over the western and eastern Pacific in addition to the central Pacific. The identification of CP ENSO-related SSTA patterns will help improve the prediction of WNP TC activity.

Our study finds that the significant positive correlation between CP ENSO and WNP TC frequency widely documented in previous publications only exists on decadal timescales. There is a weak and insignificant relationship between CP ENSO and WNP TC frequency when removing the decadal component. Similar conclusions were discussed in Liu *et al*. (2019), who reported that the statistical relationship between PMM and WNP TC genesis frequency over the southeastern WNP was dominated by their co-variability on decadal timescales. One caveat of our study is that our results are derived from a statistical analysis of a limited number of samples. These main findings will be verified by numerical sensitivity experiments using different SSTA forcings in future work.

ACKNOWLEDGEMENTS

This work was jointly funded by the National Natural Science Foundation of China (61827901, 42175007, 41905001 and 42192552) and the China Postdoctoral Science Foundation (2020M680789). Klotzbach would like to acknowledge financial support from G. Unger Vetlesen Foundation.

FUNDING INFORMATION

National Natural Science Foundation of China, Grant Numbers: 61827901, 42175007, 41905001 and 42192552; China Postdoctoral Science Foundation, Grant Number: 2020M680789; G. Unger Vetlesen Foundation.

DATA AVAILABILITY STATEMENT

All data used in this study are freely available online. Western North Pacific TC best track data provided in IBTrACS are available at: https://doi.org/10.25921/82ty-9e16. Monthly mean SST data provided by the Hadley Centre Sea Ice and Sea Surface Temperature (HadISST) are obtained from: https://www.metoffice.gov.uk/hadobs/hadisst/data/download.html. The fifth generation European Centre for Medium–Range Weather Forecasts atmospheric reanalysis of the global climate (ERA5) is retrieved from: https://cds.

climate.copernicus.eu/cdsapp#!/dataset/reanalysis-era5-pressure-levels-monthly-means?tab=form.

ORCID

Jinjie Song https://orcid.org/0000-0003-3948-8894

REFERENCES

Ashok, K., Behera, S.K., Rao, S.A., Weng, H. and Yamagata, T. (2007) El Niño Modoki and its possible teleconnections. *Journal of Geophysical Research*, 112, C11007.

Bretherton, C.S., Widmann, M., Dymnikov, V.P., Wallace, J.M. and Blade, I. (1999) The effective number of spatial degrees of freedom of a time-varying field. *Journal of Climate*, 12, 1990–2009.

Cai, Y., Han, X., Zhao, H., Klotzbach, P.J., Wu, L., Raga, G.B. and Wang, C. (2022) Enhanced predictability of rapidly intensifying tropical cyclones over the western North Pacific associated with snow depth changes over the Tibetan Plateau. *Journal of Climate*, 35, 2093–2110.

Capotondi, A., Wittenberg, A.T., Newman, M., Di Lorenzo, E., Yu, J., Braconnot, P., Cole, J., Dewitte, B., Giese, B., Guilyardi, E., Jin, F., Karnauskas, K., Kirtman, B., Lee, T., Schneider, N., Xue, Y. and Yeh, S. (2015) Understanding ENSO diversity. *Bulletin of the American Meteorological Society*, 96, 921–938.

Chan, J.C.L. (1985) Tropical cyclone activity in the Northwest Pacific in relation to the El Niño/Southern Oscillation phenomenon. *Monthly Weather Review*, 113, 599–606.

Chan, J.C.L. (2000) Tropical cyclone activity over the western North Pacific associated with El Niño and La Niña events. *Journal of Climate*, 13, 2960–2972.

Chen, G. and Tam, C.-Y. (2010) Different impacts of two kinds of Pacific Ocean warming on tropical cyclone frequency over the western North Pacific. *Geophysical Research Letters*, 37, L01803.

Emanuel, K. (2018) 100 years of progress in tropical cyclone research. *Meteorological Monographs*, 59, 15.1–15.68.

Hersbach, H., Bell, B., Berrisford, P., Hirahara, S., Horányi, A., Muñoz-Sabater, J., Nicolas, J., Peubey, C., Radu, R., Schepers, D., Simmons, A., Soci, C., Abdalla, S., Abellan, X., Balsamo, G., Bechtold, P., Biavati, G., Bidlot, J., Bonavita, M., Chiara, G., Dahlgren, P., Dee, D., Diamantakis, M., Dragani, R., Flemming, J., Forbes, R., Fuentes, M., Geer, A., Haimberger, L., Healy, S., Hogan, R.J., Hólm, E., Janisková, M., Keeley, S., Laloyaux, P., Lopez, P., Lupu, C., Radnoti, G., Rosnay, P., Rozum, I., Vamborg, F., Villaume, S. and Thépaut, J. (2020) The ERA5 global reanalysis. *Quarterly Journal of the Royal Meteorological Society*, 146, 1999–2049.

Hsu, P., Ho, C., Liang, S. and Kuo, N. (2013) Impacts of two types of El Niño and La Niña events on typhoon activity. *Advances in Meteorology*, 2013, 632470.

Jeong, H.-I. and Ahn, J.-B. (2017) A new method to classify ENSO events into eastern and central Pacific types. *International Journal of Climatology*, 37, 2193–2199.

Kao, H. and Yu, J. (2009) Contrasting eastern-Pacific and central-Pacific types of ENSO. *Journal of Climate*, 22, 615–632.

Kim, H.-M., Webster, P.J. and Curry, J.A. (2011) Modulation of North Pacific tropical cyclone activity by three phases of ENSO. *Journal of Climate*, 24, 1839–1849.

Knapp, K.R., Kruk, M.C., Levinson, D.H., Diamond, H.J. and Neuman, C.J. (2010) The International Best Track Archive for Climate Stewardship (IBTrACS). *Bulletin of the American Meteorological Society*, 91, 363–376.

Kug, J.-S., Choi, J., An, S.-I., Jin, F.-F. and Wittenberg, A.T. (2010) Warm pool and cold tongue El Niño events as simulated by the GFDL CM2.1 coupled GCM. *Journal of Climate*, 23, 1226–1239.

Lander, M.A. (1994) An exploratory analysis of the relationship between tropical storm formation in the western North Pacific and ENSO. *Monthly Weather Review*, 122, 636–651.

Li, C. and Wang, C. (2014) Simulated impacts of two types of ENSO events on tropical cyclone activity in the western North Pacific: large-scale atmospheric response. *Climate Dynamics*, 42, 2727–2743.

Li, R.C.Y. and Zhou, W. (2012) Changes in western Pacific tropical cyclones associated with the El Niño–Southern Oscillation cycle. *Journal of Climate*, 25, 5864–5878.

Li, X., Cheng, X., Fei, J., Huang, X. and Ding, J. (2022) The modulation effect of sea surface cooling on the eyewall replacement cycle in Typhoon Trami (2018). *Monthly Weather Review*, 150, 1417–1436.

Liang, Z., Ding, J., Fei, J., Cheng, X. and Huang, X. (2021) Direct/indirect effects of aerosols and their separate contributions to Typhoon Lupit (2009): eyewall versus peripheral rainbands. *Science China Earth Sciences*, 64, 2113–2128.

Liu, C., Zhang, W., Stuecker, M.F. and Jin, F.-F. (2019) Pacific meridional mode-western North Pacific tropical cyclone linkage explained by tropical Pacific quasi-decadal variability. *Geophysical Research Letters*, 46, 13346–13354.

Liu, Y. and Chen, G. (2018) Intensified influence of the ENSO Modoki on boreal summer tropical cyclone genesis over the western North Pacific since the early 1990s. *International Journal of Climatology*, 38(Suppl. 1), e1258–e1265.

Ma, Z. and Fei, J. (2022) A comparison between moist and dry tropical cyclones: the low effectiveness of surface sensible heat flux in storm intensification. *Journal of the Atmospheric Sciences*, 79, 31–49.

Patricola, C.M., Camargo, S.J., Klotzbach, P.J., Saravanan, R. and Chang, P. (2018) The influence of ENSO flavors on western North Pacific tropical cyclone activity. *Journal of Climate*, 31, 5395–5416.

Rayner, N.A., Parker, D.E., Horton, E.B., Folland, C.K., Alexander, L.V., Rowell, D.P., Kent, E.C. and Kaplan, A. (2003) Global analyses of sea surface temperature, sea ice, and night marine air temperature since the late nineteenth century. *Journal of Geophysical Research*, 108, 4407.

Ren, H.-L. and Jin, F.-F. (2011) Niño indices for two types of ENSO. *Geophysical Research Letters*, 38, L04704.

Saunders, M.A., Chandler, R.E., Merchant, C.J. and Roberts, F.P. (2000) Atlantic hurricanes and NW Pacific typhoons: ENSO spatial impacts on occurrence and landfall. *Geophysical Research Letters*, 27, 1147–1150.

Song, J. and Klotzbach, P.J. (2018) What has controlled the poleward migration of annual averaged location of tropical cyclone lifetime maximum intensity over the western North Pacific since 1961? *Geophysical Research Letters*, 45, 1148–1156.

Song, J. and Klotzbach, P.J. (2019) Relationship between the Pacific–North American pattern and the frequency of tropical

cyclones over the western North Pacific. *Geophysical Research Letters*, 46, 6118–6127.

Song, J., Klotzbach, P.J. and Duan, Y. (2021) Recent weakening of the interannual relationship between ENSO Modoki and boreal summer tropical cyclone frequency over the western North Pacific. *Journal of the Meteorological Society of Japan*, 99, 1071–1088.

Stuecker, M.F. (2018) Revisiting the Pacific meridional mode. *Scientific Reports*, 8, 3216.

Sullivan, A., Luo, J.-J., Hirst, A.C., Bi, D., Cai, W. and He, J. (2016) Robust contribution of decadal anomalies to the frequency of central-Pacific El Niño. *Scientific Reports*, 6, 38540.

Takahashi, K., Montecinos, A., Goubanova, K. and Dewitte, B. (2011) ENSO regimes: reinterpreting the canonical and Modoki El Niño. *Geophysical Research Letters*, 38, L10704.

Timmermann, A., An, S.I., Kug, J.S., Jin, F.F., Cai, W., Capotondi, A., Cobb, K.M., Lengaigne, M., McPhaden, M.J., Stuecker, M.F., Stein, K., Wittenberg, A.T., Yun, K.S., Bayr, T., Chen, H.C., Chikamoto, Y., Dewitte, B., Dommenget, D., Grothe, P., Guilyardi, E., Ham, Y.G., Hayashi, M., Ineson, S., Kang, D., Kim, S., Kim, W., Lee, J.Y., Li, T., Luo, J.J., McGregor, S., Planton, Y., Power, S., Rashid, H., Ren, H.L., Santoso, A., Takahashi, K., Todd, A., Wang, G., Wang, G., Xie, R., Yang, W.H., Yeh, S.W., Yoon, J., Zeller, E. and Zhang, X. (2018) El Niño–Southern Oscillation complexity. *Nature*, 559, 535–545.

Wang, B. and Chan, J.C.L. (2002) How strong ENSO events affect tropical storm activity over the western North Pacific. *Journal of Climate*, 15, 1643–1658.

Wang, C., Li, C., Mu, M. and Duan, W. (2013) Seasonal modulations of different impacts of two types of ENSO events on tropical cyclone activity in the western North Pacific. *Climate Dynamics*, 40, 2887–2902.

Wang, C. and Wang, X. (2013) Classifying El Niño Modoki I and II by different impacts on rainfall in southern China and typhoon tracks. *Journal of Climate*, 26, 1322–1338.

Yeh, S.-W., Kug, J.-S., Dewitte, B., Kwon, M.-H., Kirtman, B. and Jin, F.-F. (2009) El Niño in a changing climate. *Nature*, 461, 511–514.

Zhang, W., Leung, Y. and Fraedrich, K. (2015) Different El Niño types and intense typhoons in the western North Pacific. *Climate Dynamics*, 44, 2965–2977.

Zhao, H., Lu, Y., Jiang, X., Klotzbach, P.J., Wu, L. and Cao, J. (2022a) A statistical intraseasonal prediction model of extended boreal summer western North Pacific tropical cyclone genesis. *Journal of Climate*, 35, 2459–2478.

Zhao, H., Zhao, K., Klotzbach, P.J., Wu, L. and Wang, C. (2022b) Interannual and interdecadal drivers of meridional migration of western North Pacific tropical cyclone lifetime maximum intensity location. *Journal of Climate*, 35, 2709–2722.

How to cite this article: Song, J., Klotzbach, P. J., Wei, N., & Duan, Y. (2023). Modulation of western North Pacific tropical cyclone formation by central Pacific El Niño–Southern Oscillation on decadal and interannual timescales. *International Journal of Climatology*, *43*(1), 426–437. https://doi.org/10.1002/joc.7777